ACS OMEGA

http://pubs.acs.org/journal/acsodf

Article

Design, Synthesis, and Antifungal Activity of Novel Longifolene-Derived Diacylhydrazine Compounds

Shuyan Zhao, Guishan Lin,* Wengui Duan,* Qianan Zhang, Yinglan Huang, and Fuhou Lei

Cite This: *ACS Omega* 2021, 6, 9104–9111

Read Online

ACCESS | Metrics & More | Article Recommendations | Supporting Information

ABSTRACT: Succinate dehydrogenase (SDH) present in the inner mitochondrial membrane is an important target enzyme for the design of SDH inhibitor-type fungicides. Using SDH as the target enzyme, 22 novel longifolene-derived diacylhydrazine compounds were designed and synthesized using the renewable natural product longifolene as the starting material. Their structures were confirmed by IR, ^{1}H NMR, ^{13}C NMR, electrospray mass spectrometry, and elemental analysis. In vitro antifungal activity of the target compounds was preliminarily evaluated. As a result, some of them showed better or comparable antifungal activity than that of the commercial fungicide chlorothalonil, in which compound **5a** had inhibitory rates of 97.5, 80.5, 72.1, and 67.1% against *Physalospora piricola*, *Colletotrichum orbiculare*, *Alternaria solani*, and *Gibberella zeae*, respectively, presenting excellent and broad-spectrum activity that deserved further study. Besides, a reasonable and effective three-dimensional structure−activity quantitative relationship model has been established. There was a significant positive correlation between the antifungal activity and the docking-based binding energy analyzed using Spearman's rank correlation algorithm. Also, the simulative binding pattern of the target compounds with SDH was investigated by molecular docking study. Furthermore, the diacylhydrazine and phenol groups of the target compounds were proposed to be the potential pharmacophores by frontier molecular orbital analysis.

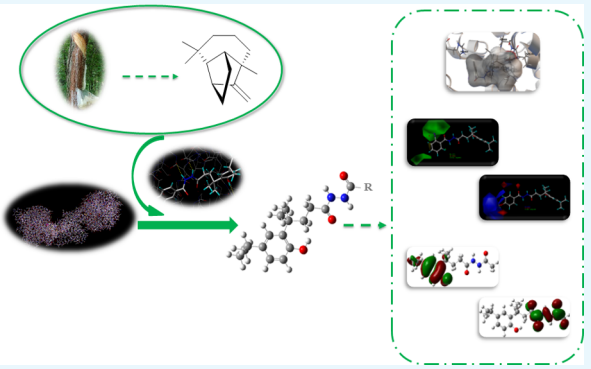

INTRODUCTION

The number of commercial succinate dehydrogenase (or succinate-ubiquinone oxidoreductase, EC 1.3.5.1) inhibitor (SDHI) fungicides has been increasing in recent years because of their highly effective and broad-spectrum fungicidal performance, which was owing to their unique action mode with the target enzyme.[1] At present, about 20 SDHI fungicides have been registered according to the statistics from the Fungicide Resistance Action Committee including carboxin, fluxapyroxad, boscalid, benzovindiflupyr, bixafen, penflufen, and so forth.[2] All of these compounds are carboxamides. Meanwhile, fruitful research studies for discovering novel succinate dehydrogenase (SDH) inhibitor molecules have been performed incessantly,[3−8] and some other pharmacophore-type compounds for SDHI fungicides have been found such as carbohydrazides[9] and sulfonamides.[10]

SDH is the only enzyme involved in both the respiratory chain and the tricarboxylic acid cycle. It catalyzes the oxidation of succinate to fumarate, coupled with the reduction of ubiquinone to ubiquinol in the inner mitochondrial membrane. It has been identified as a significant target for the design of agrochemical fungicides.[11,12] The kinetics research of SDH inhibition through 10 commercial carboxamide fungicides provided the useful reference for the design of new SDHI fungicides. The result showed that the carboxamide molecule competed with ubiquinone rather than succinate, and the carbonyl oxygen atom of the carboxamide formed hydrogen bonds with two key amino acid residues TRP and TYR, the acid moiety interacted with the residues ARG, SER, IIE, and PRO, and the amine moiety interacted with the residues TRP, IIE, and IIE.[13]

We also noted that diacylhydrazine compounds containing double carboxamide groups exhibited diverse pharmacological properties, such as insecticidal,[14] herbicidal,[15] antifungal,[16] antitumor,[17,18] and antimalarial[19] activities. Meanwhile, compounds bearing a phenol pharmacophore comparable to ubiquinol showed a wide range of biological activities, especially antifungal activity.[20−22]

On the other hand, longifolene (4,8,8-trimethyl-9-methylenedecahydro-1,4-methanoazulene), a naturally occurring tricyclic sesquiterpene, is the main constituent of heavy turpentine, which is a byproduct in the production of rosin

Received: January 13, 2021
Accepted: March 9, 2021
Published: March 24, 2021

https://doi.org/10.1021/acsomega.1c00217
ACS Omega 2021, 6, 9104−9111

and turpentine from living pine trees, but just used as a less expensive boiler fuel.[23] By the isomerization−aromatization reaction, longifolene can be converted into 7-isopropyl-1, 1-dimethyltetralin (longifolene-derived tetraline),[24] whose structural modification was explored to be used in perfume[25] or medicine[26] and so forth. In light of these clues above and as the continuation of our interest in the work of high value-added application of forest resources for the sustainable development of the resin industy,[26−30] a series of novel longifolene-derived diacylhydrazine compounds incorporating phenol and diacylhydrazine groups were designed by the strategy of molecular docking-based virtual screening based on the crystal structure of SDH (UniProtKB AC P32420, homology modeling on SWISS-MODEL web) and synthesized and characterized. In vitro antifungal activity of all the target compounds was preliminarily evaluated against eight fungi. Furthermore, a three-dimensional structure−activity quantitative relationship (3D-QSAR) model was built by the comparative molecular field analysis (CoMFA) method, molecular docking was conducted to explore the binding mode for these molecules with SDH, and the frontier molecular orbital was calculated to analyze the potential pharmacophore for the target molecules.

RESULTS AND DISCUSSION

Synthesis and Characterization of Compounds. The target compounds were synthesized according to the route shown in Scheme 1. Longifolene-derived tetralin **2** was prepared by the isomerization−aromatization reaction using nanocrystalline sulfated zirconia as a catalyst and further oxidized by TBHP oxidant to give longifolene-derived tetralone **3**. Compound **2** and **3** were prepared according to our previous report.[25] Compound **4** was prepared by the Baeyer−Villager oxidation reaction using *m*-CPBA as the oxidant. 22 longifolene-derived diacylhydrazine compounds **5a−5v** were then synthesized by the hydrazinolysis reaction of compound **4** with different substituted acylhydrazine compounds in 75.0−80.0% yields.

Scheme 1. Synthetic Route of the Longifolene-Derived Diacylhydrazine Compounds 5a−5v (Table 1)[a]

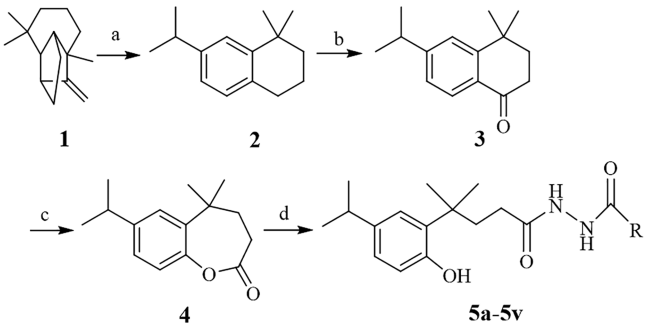

[a]Reagents and conditions: (a) $ZnCl_2$, 140.0 °C, reflux 8 h; (b) TBHP, CH_3CN, $CuCl_2$, 40.0 °C; (c) *m*-CPBA, Cl_2Cl_2, rt; and (d) EtOH, a series of different acylhydrazine compounds, 78.0 °C.

The structures of the target compounds were confirmed by IR, NMR, electrospray mass spectrometry (ESI-MS), and elemental analysis. In the IR spectra, the characteristic absorption bands at about 3438−3318 and 3289−3187 cm^{-1} were attributed to the stretching vibrations of the O−H and N−H, respectively. The characteristic absorption bands at about 1706−1661 cm^{-1} were assigned to the stretching vibrations of C═O. The ^1H NMR spectra exhibited characteristic signals at δ 6.93−6.69 ppm, which were assigned to the protons of the benzene ring, and the characteristic signals at about δ 10.21−8.88 ppm were assigned to the amino protons of the diacylhydrazine moiety. The ^{13}C NMR spectra of the target compounds showed peaks for two carbon atoms of C═O at δ 173.94−163.23 ppm and carbon atoms of the benzene ring at δ 146.11−116.38 ppm. The other saturated carbons displayed signals in the region of δ 37.60−24.81 ppm. Their molecular weights and the C, H, and N elemental ratios agreed with the results of ESI-MS and elemental analysis, respectively.

In Vitro Antifungal Activity. The antifungal activities of the target compounds **5a−5v** were evaluated by the agar dilution method[31] against eight plant pathogens at 50 mg/L, including apple root spot (*Physalospora piricola*), wheat scab (*Gibberella zeae*), speckle on peanut (*Cercospora arachidicola*), tomato early blight (*Alternaria solani*), fusarium wilt on cucumber (*Fusarium oxysporum f. sp. Cucumerinum*), watermelon anthracnose (*Colletotrichum orbiculare*), corn southern leaf blight (*Bipolaris maydis*), and rice sheath blight (*Rhizoctonia solani*). The commercial fungicide chlorothalonil was used as a positive control. The results are listed in Table 2. It was found that most of the tested compounds displayed certain antifungal activity against the tested fungi. Compared with that of the commercial fungicide (chlorothalonil), some compounds exhibited excellent antifungal activity. For instance, compound **5a** (R = *o*-I Ph) had inhibitory rates of 97.5, 80.5, 72.1, and 67.1% against *P. piricola*, *C. orbiculare*, *A. solani*, and *G. zeae*, respectively, presenting better antifungal effect than that of the positive control with inhibitory rates of 92.9, 75.0, 45.0, and 58.3%, respectively. Besides, compounds **5s** (R = *o*-Cl Ph), **5j** (R = *o*-NO_2 Ph), **5d** (R = *p*-OCH_3 Ph), and **5g** (R = *p*-F Ph) had inhibitory rates of 97.5, 87.1, 80.8, and 80.8%, respectively, against *P. piricola*, **5h** (R = *o*-F Ph) had an inhibitory rate of 70.8% against *G. zeae*, **5k** (R = *o*-Cl

Table 1. R Groups of the Compounds 5a−5v

compounds	R	compounds	R	compounds	R
5a	*o*-I Ph	**5i**	*o*-CF_3 Ph	**5q**	*p*-$C(CH_3)_3$ Ph
5b	2,4-OH Ph	**5j**	*o*-NO_2 Ph	**5r**	Ph
5c	*o*-OH Ph	**5k**	*o*-Cl Ph	**5s**	CH_3
5d	*p*-OCH_3 Ph	**5l**	*m*-Cl Ph	**5t**	CH_2 Ph
5e	*o*-Br Ph	**5m**	*p*-Cl Ph	**5u**	CH_2CN
5f	*p*-Br Ph	**5n**	*p*-CH_3 Ph	**5v**	α-furyl
5g	*p*-F Ph	**5o**	*o*-CH_3 Ph		
5h	*o*-F Ph	**5p**	*p*-CH_2OH Ph		

https://doi.org/10.1021/acsomega.1c00217
ACS Omega 2021, 6, 9104−9111

Table 2. In Vitro Antifungal Activity of the Target Compounds 5a−5v

		relative inhibitory rate (%)							
compounds	R	*P. piricola*	*G. zeae*	*C. arachidicola*	*A. solani*	*F. oxysporum* f. sp. *Cucumerinum*	*C. orbiculare*	*B. maydis*	*R. solani*
5a	*o*-I Ph	97.5	67.1	58.1	72.1	76.0	80.5	65.0	44.1
5b	2,4-OH Ph	70.4	52.9	69.3	68.6	44.0	41.8	40.0	73.5
5c	*o*-OH Ph	42.9	70.7	69.7	54.8	65.3	46.4	57.5	14.7
5d	*p*-OCH_3 Ph	80.8	45.7	69.3	51.4	56.8	62.3	57.5	18.2
5e	*o*-Br Ph	74.6	56.4	61.9	58.3	67.4	55.5	60.0	0
5f	*p*-Br Ph	51.7	52.9	54.4	51.4	48.3	48.6	45.0	41.8
5g	*p*-F Ph	80.8	52.9	58.1	47.9	50.4	53.2	60.0	26.5
5h	*o*-F Ph	53.8	70.8	54.4	51.4	48.3	50.9	42.5	0
5i	*o*-CF_3 Ph	51.3	70.7	61.9	54.8	65.3	41.8	60.0	22.9
5j	*o*-NO_2 Ph	87.1	52.9	54.4	54.8	56.8	55.5	55.0	0
5k	*o*-Cl Ph	47.4	70.7	65.6	72.1	39.8	62.3	52.5	0
5l	*m*-Cl Ph	55.8	74.3	50.7	54.8	58.9	57.7	55.0	0
5m	*p*-Cl Ph	47.5	70.7	58.1	44.5	58.9	48.6	60.0	0
5n	*p*-CH_3 Ph	76.3	38.6	39.6	47.9	56.8	50.9	50.0	31.2
5o	*o*-CH_3 Ph	62.1	56.4	50.7	54.8	52.6	53.2	50.0	0
5p	*p*-CH_2OH Ph	56.4	56.4	69.3	54.8	37.7	46.4	35.0	20.6
5q	*p*-$C(CH_3)_3$ Ph	32.9	70.7	61.9	51.4	35.5	30.5	32.5	0
5r	Ph	45.4	74.3	50.7	51.4	35.5	37.3	27.5	0
5s	CH_3	97.5	60.0	58.1	61.7	44.0	46.4	32.5	0
5t	CH_2 Ph	70.0	70.7	65.6	44.5	50.4	53.2	45.0	0
5u	CH_2CN	46.7	60.0	50.7	61.7	50.4	44.1	40.0	0
5v	*α*-furyl	45.4	35.0	58.1	51.4	50.4	46.4	40.0	14.7
chlorothalonil		92.9	58.3	94.4	45.0	91.7	75.0	81.8	96.3

Ph) had an inhibitory rate of 72.1% against *A. solani*, and **5b** (R = 2,4-OH Ph) had an inhibitory rate of 73.5% against *R. solani*, showing excellent to moderate antifungal activity. Overall, compound **5a** (R = *o*-I Ph) exhibited excellent and broad-spectrum antifungal activity against most of the tested fungi. It was also found that the R groups had a noticeable influence on activity, so a 3D-QSAR study was performed subsequently.

3D-QSAR Analysis. 3D-QSAR analysis of the experimental and predicted antifungal activity against *P. piricola* for the target compounds was carried out by the CoMFA method according to our previous report,[32] and the 16 target compounds in the training set and the 2 target compounds in the test set are presented in Table 3. The result is shown in Table 4. A 3D-QSAR model was established with the conventional correlation r^2 = 0.997 and the cross-validated coefficient q^2 = 0.574. Referring to the report,[33] the inhibitory rate against *P. piricola* was converted to an active factor (AF). The scatter plot of the predicted AF values versus experimental AF values is presented in Figure 1, where all data were concentrated near the $X = Y$ line, illustrating that the 3D-QSAR model was reliable and had a good predictive ability.

The contribution rates for steric and electrostatic fields were 68.2 and 31.8% (Table 4), respectively, showing that the steric field was the major contributor to the increase in activity. The steric and electrostatic field contour maps for the R groups at the benzene ring are presented in Figure 2. The field contours were represented with different colors: In the steric contour map, the green enclosed volume represented that the R group embedding this area will favor the increase in activity, while yellow defines the opposite. In the electrostatic contour map, the blue enclosed volume represented that the R group with an electropositive surface embedding in this area will favor the increase in activity, while red defines the opposite. As shown in Figure 2, a green block is suspended above the 2-position of the benzene ring and a blue block is around the 4-position.

Table 3. AF Values of Experimental and Predicted Activities for the Target Compounds 5a−5r[a]

compounds	R	MW	AF	AF′	residual
5a	*o*-I Ph	494.11	−1.103	−1.148	0.045
5b	2,4-OH Ph	400.20	−2.226	−2.228	0.002
5c	*o*-OH Ph	384.20	−2.709	−2.725	0.016
5d	*p*-OCH_3 Ph	398.22	−1.976	−1.987	0.011
5e	*o*-Br Ph	446.12	−2.182	−2.066	−0.116
5f	*p*-Br Ph	446.12	−2.620	−2.655	0.035
5g	*p*-F Ph	386.20	−1.963	−1.956	−0.007
5h	*o*-F Ph	386.20	−2.521	−2.509	−0.012
5i	*o*-CF_3 Ph	436.20	−2.617	−2.615	−0.002
5j	*o*-NO_2 Ph	413.20	−1.787	−1.800	0.013
5k	*o*-Cl Ph	402.17	−2.650	−2.709	0.059
5l	*m*-Cl Ph	402.17	−2.503	−2.505	0.002
5m	*p*-Cl Ph	402.17	−2.648	−2.626	−0.022
5n	*p*-CH_3 Ph	382.23	−2.075	−2.076	−0.001
5o	*o*-CH_3 Ph	382.23	−2.368	−2.358	−0.010
5p	*p*-CH_2OH Ph	398.22	−2.488	−2.496	0.008
5q*	*p*-$C(CH_3)_3$ Ph	424.27	−2.937	−2.930	−0.007
5r*	Ph	368.21	−2.647	−2.622	−0.025

[a]AF: experimental value; AF′: predicted value; *: test set compounds.

Table 4. Summary of CoMFA

					contribution (%)	
	q^2	r^2	*S*	*F*	steric	electrostatic
CoMFA	0.574	0.997	0.045	105.314	0.682	0.318

Namely, the introduction of R groups embedding the green enclosed volume will favor the increase of activity, but cannot in the opposite. For example, as shown in Figure 2a, compound **5a** (R = *o*-I Ph), of which the iodine atom can embed in the green block (Figure 2b), showed higher activity

https://doi.org/10.1021/acsomega.1c00217
ACS Omega 2021, 6, 9104−9111

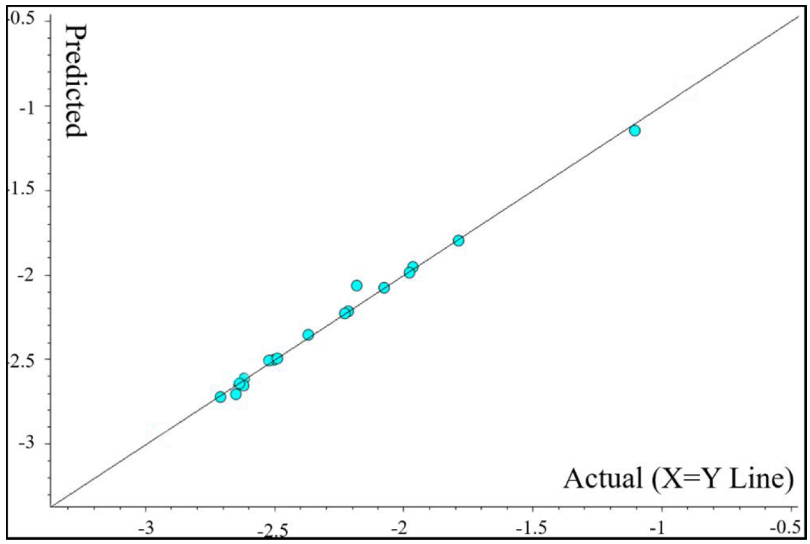

Figure 1. Scatter plot of predicted AF values vs experimental AF values.

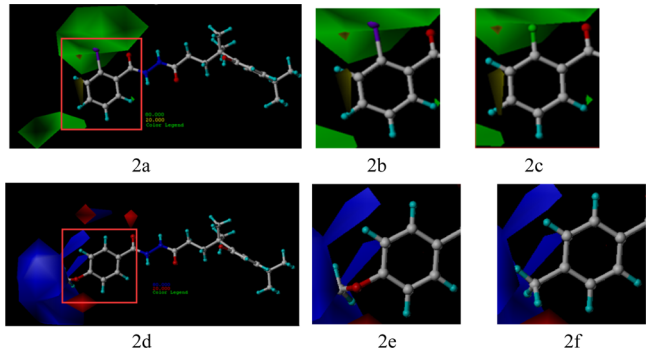

Figure 2. Contours of CoMFA: (a) contour of the steric contribution represented in yellow and green, (b) expanded contour of compound **5a**, (c) expanded contour of compound **5k**, (d) contour of electrostatic contribution represented in red and blue, (e) expanded contour of compound **5d**, and (f) expanded contour of compound **5n**.

than compound **5k** (R = *o*-Cl Ph), of which the chlorine atom cannot embed in the green block (Figure 2c). Likewise, as shown in Figure 2d, compound **5d** (R = p-OCH_3 Ph), which had a methoxy group with an electropositive surface located at the 4-position of the benzene ring (Figure 2e), showed better antifungal activity than compound **5n** (R = p-CH_3 Ph, Figure 2f). Other compounds shared a similar case.

Molecular Docking and Frontier Molecular Orbital. The molecular docking study for the target compounds was performed using AutoDock 4.2.6 software[34] according to our previous work.[26] The simulation of the binding pattern for the best antifungal activity of compound **5a** and commercial SDHI carboxin with SDH is shown in Figure 3. The oxygen atoms of carbonyl and phenol moieties interacted with the residues TRP173 and HIS60 via the H bond (Figure 3a), which are similar to the commercial SDHI carboxin (Figure 3b). Besides, compound **5a** was surrounded by the hydrophobic residues HIS104, VAL59, and TYR58.

In fact, some diacylhydrazine compounds were used as commercial pesticides such as tebufenozide, chromafenozide, and methoxyfenozide, which were ecdysone receptor agonists. Therefore, molecular docking investigation for the comparison between the target compound **5a** and the commercial pesticide tebufenozide was carried out using the heterodimer ecdysteroid receptor/ultraspiracle (EcR/USP) as the target protein

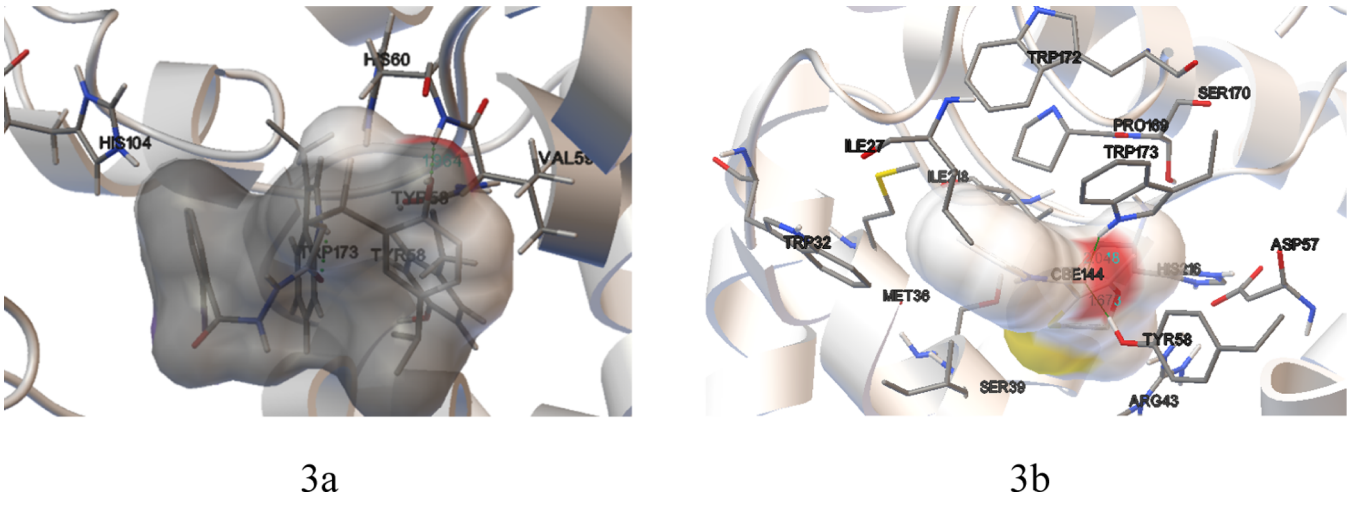

Figure 3. Binding mode and the interaction of (a) compound **5a** with SDH and (b) commercial SDHI carboxin with SDH.

https://doi.org/10.1021/acsomega.1c00217
ACS Omega 2021, 6, 9104−9111

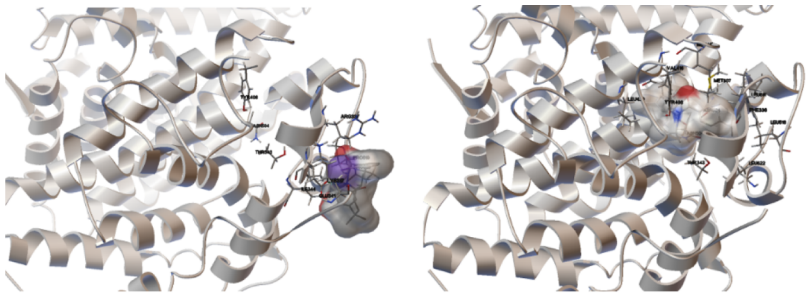

4a 4b

Figure 4. Binding mode and the interaction of (a) compound **5a** with EcR/USP and (b) tebufenozide with EcR/USP.

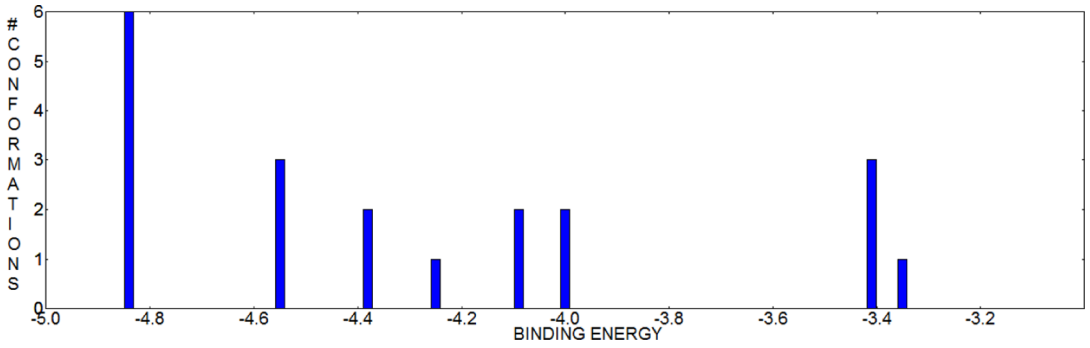

Figure 5. Cluster of 20 docked conformations for compound **5a**.

(PDB ID 1R20). The result is shown in Figure 4. As a whole, compound **5a** embeds incompletely in the ligand (chromafenozide)-binding domain (Figure 4a), while the tebufenozide showed the opposite (Figure 4b), implying that compound **5a** showed a potentially weak action with EcR/USP.

Meanwhile, the correlation between the binding energy and antifungal activity was evaluated. There were 20 conformations docked for each target compound (Figure 5), and the lowest binding energy in the maximum cluster for the docked conformations was chosen as the representative binding energy for the corresponding compound. The scatter plot of AF values versus binding energies for the title compounds is shown in Figure 6. All of the data were concentrated near the line $Y = 0.3066X - 0.8523$, illustrating that there was a clear positive monotonic association between AF values and binding energies. In addition, Spearman's rank correlation coefficient analytical approach was carried out using IBM SPSS STATITICS 22 software to investigate the correlation between AF values and binding energies. The result is listed in Table 5.

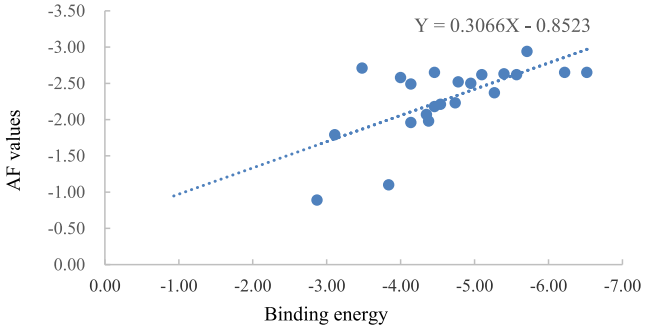

Figure 6. Monotonicity of AF values vs binding energies for the target compounds.

Table 5. Spearman Rank Correlation Coefficient of AF Values Versus Binding Energies for the Target Compounds

		binding energy	AF values
binding energy	correlation coefficient	1.000	0.762
	Sig. (1-tailed)		0.001
AF values	correlation coefficient	0.762	1.000
	Sig. (1-tailed)	0.001	

It was found that the correlation was significant at 0.001 (at 0.01 level). The Spearman correlation coefficient was 0.762, indicating that there was a significant positive correlation, namely, the activity gradually increased with the increase in binding energies.

According to frontier molecular orbital theory, the highest occupied molecular orbital (HOMO) and the lowest unoccupied molecular orbital (LUMO) are the two important factors affecting the bioactivity of compounds, because the HOMO has the priority to provide electrons, while the LUMO easily accepts electrons. The group with frontier molecular orbitals was a potential pharmacophore.[35] Therefore, the frontier molecular orbitals of compound **5s** with good inhibitory activity were calculated using the mean of the DFT/B3LYP method in the Gaussian 09 package.[36] The total energy of compound **5s** was −998.65190379 a.u., and the energy gap between the HOMO and LUMO was 0.217 a.u. The DFT-derived graphic results are presented using GaussView 5 software[37] in Figure 7. The HOMO is located on the phenol moiety and the LUMO is located on the diacylhydrazine moiety, implying that these moieties were potential pharmacophores for the contribution of bioactivity.

CONCLUSIONS

In summary, 22 novel longifolene-derived diacylhydrazine compounds were designed by molecular docking-based virtual

https://doi.org/10.1021/acsomega.1c00217
ACS Omega 2021, 6, 9104−9111

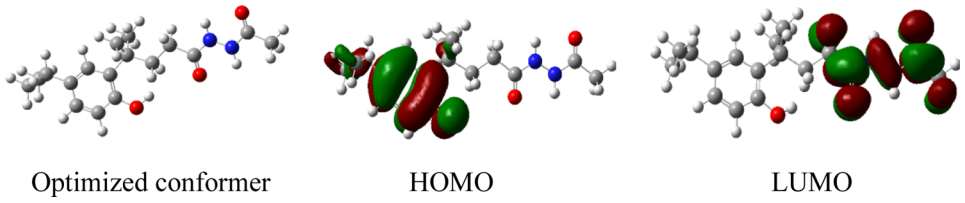

Figure 7. Optimized conformer and the maps of HOMO and LUMO for compound **5s**.

screening based on the crystal structure of SDH, synthesized using the renewable natural forest product longifolene as the starting material, and confirmed by IR, ^{1}H NMR, ^{13}C NMR, ESI-MS, and elemental analysis. The evaluation of the in vitro antifungal activity for the target compounds showed that some of them exhibited excellent inhibitory activity against the tested fungi. Meanwhile, a reasonable and effective 3D-QSAR model has been established for the further study of these types of compounds. There was a significant positive Spearman's rank correlation between the antifungal activity and the docking-based binding energy. Molecular docking study revealed that there were H bonds and hydrophobic interactions between diacylhydrazine compounds and SDH. The distributed situation of the frontier molecular orbital showed that the phenol and diacylhydrazine moieties were potential pharmacophores for the contribution of bioactivity. Overall, compound **5a** with excellent and broad-spectrum activity was the potential SDHI leading compound worthy of further study.

MATERIALS AND METHODS

Synthesis and Characterization of Compounds. The synthesized compounds were characterized by IR (Nicolet IS 50 FT-IR spectrometer using KBr tableting), ^{1}H NMR and ^{13}C NMR (Bruker AVANCE III HD 600 MHz spectrometer using $CDCl_3$ or dimethyl sulfoxide as the solvent and TMS as an internal standard), ESI-MS (TSQ Quantum Access MAX HPLC-MS apparatus), and elemental analysis (PerkinElmer 2400II elemental analyzer). The melting points were measured using a Hanon MP420 automatic melting point apparatus. All the characterization data above can be found in the Supporting Information. Longifolene **1** was provided by Wuzhou Pine Chemicals Co., Ltd., Wuzhou, China (65.0%, GC analyses). All other reagents were purchased from commercial suppliers and used as received. Using longifolene as the starting material, the longifolene-derived diacylhydrazine target compounds were synthesized. The longifolene-derived tetraline **2** and the longifolene-derived tetralone **3** were prepared according to our previously reported method.

General Procedure for the Synthesis of Compound 4. Compound **3** (1.00 g, 9.25 mmol) and *m*-CPBA (3.19 g, 18.50 mmol) were mixed in CH_2Cl_2 (5 mL). The mixture was continuously stirred at room temperature. After the completion of the reaction, monitored by the thin layer chromatography method, the resulting mixture was washed three times with 5.0% $NaHCO_3$ aqueous solution. The organic layer was dried over anhydrous Na_2SO_4 and evaporated in a vacuum. The residue was purified by silica gel column chromatography (petroleum ether/EtOAc = 80:1, v/v) to give the colorless liquid compound **4**.

General Procedure for the Synthesis of Longifolene-Derived Diacylhydrazine Compounds 5a−5v. Under stirring, a solution of compound **4** (1.00 g, 4.31 mmol) in ethanol (5 mL) was added dropwise into the solution (5 mL) of substituted acylhydrazine compounds (12.93 mmol) in ethanol at 78.0 °C. After the completion of the reaction, monitored by the thin layer chromatography method, the reaction mixture was washed three times with 5.0% HCl aqueous solution (10 mL each time). The aqueous phase was extracted with Et_2O. The combined organic phase was concentrated under reduced pressure to obtain the crude product, which was purified by silica gel column chromatography (petroleum ether/EtOAc = 5:1, v/v) to afford the target compounds **5a−5v**.

In Vitro Antifungal Activity Test by the Agar Dilution Method. This test procedure was carried out according to the reported method and is described briefly as follows. Three copies of a culture plate containing 50 μg/mL tested compound and plant pathogenic fungi were cultured at 24.0 ± 1.0 °C for 48 h. Meanwhile, aseptic distilled water was used as a blank control. There were three replicates for each tested compound. The inhibition rate was calculated by comparing the mycelium diameter of the fungi treated with the emulsion to the blank control.

3D-QSAR Analysis. The 3D-QSAR model was built using the CoMFA method of Sybyl-X 2.1.1 software. The structures of compounds **5a−5v** were optimized based on the Tripos force field and Gasteiger-Hückel charges. Compound **5a** with the best activity was used as the template molecule and the common skeleton atoms are marked with an asterisk, as shown in Figure 8. The 18 target compounds, of which the R group

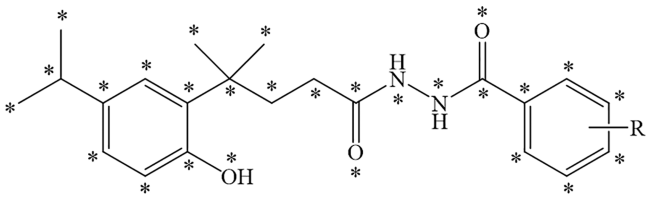

Figure 8. Common skeleton atoms marked with an asterisk.

contains the benzene ring, were superimposed and the result is displayed in Figure 9. The inhibition rate against *P. piricola* was converted to the AF using the formula: AF = log{[relative inhibitory rate/(100 − relative inhibitory rate)] × molecular weight}.

The built 3D-QSAR model was checked by the partial least-squares method. Its predictive capability was judged by a cross-validated value squared (q^2), a correlation coefficient squared (r^2), a standard deviation (S), and a Fisher validation value (F).

Molecular Docking and Frontier Molecular Orbital. The molecular docking was carried out using AutoDock 4.2.6 software. The PDB file of the target enzyme SDH−carboxin complex (UniProtKB AC P32420, homology modeling) was downloaded from the SWISS-MODEL web. The small molecules in the SDH−carboxin complex were removed. A

https://doi.org/10.1021/acsomega.1c00217
ACS Omega 2021, 6, 9104−9111

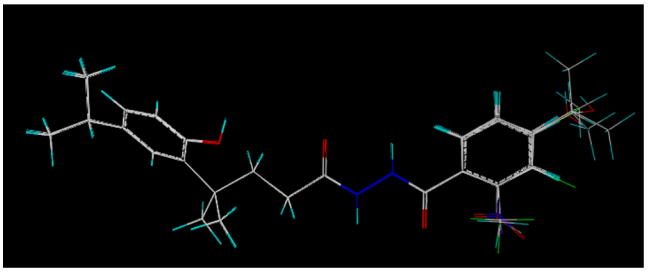

Figure 9. Superposition mode for the 18 target compounds containing the benzene ring on the R group.

60 × 60 × 60 point grid box around the Q-site was set as the docking area. The docking parameters were searched using the Lamarckian genetic algorithm (GA) and the number of GA runs was set to 20 (namely, there were 20 conformations for each compound). The lowest binding energy in the maximum cluster for the docked conformations was chosen as the representative binding energy for the corresponding compound.

Moreover, the frontier molecular orbital for the target compound **5s** was calculated by the DFTB3LYP/6-31G (d, p) method in the Gaussian 09 package on the Computer Supercomputing Platform at Guangxi University, and the result was viewed using GaussView 5 software.

■ ASSOCIATED CONTENT

Supporting Information

The Supporting Information is available free of charge at https://pubs.acs.org/doi/10.1021/acsomega.1c00217.

Structure of compounds **5a−5v**; IR, ^{1}H NMR, ^{13}C NMR, and ESI-MS analysis and spectra; model quality estimate of homology modeling on SWISS-MODEL web; and partial result of molecular docking-based virtual screening for the designed compounds (PDF)

■ AUTHOR INFORMATION

Corresponding Authors

Guishan Lin − *School of Chemistry and Chemical Engineering, Guangxi University, Nanning, Guangxi 530004, P. R. China*; Email: gslin@gxu.edu.cn

Wengui Duan − *School of Chemistry and Chemical Engineering, Guangxi University, Nanning, Guangxi 530004, P. R. China*; orcid.org/0000-0001-8140-0011; Phone: +86-771-2097058; Email: wgduan@gxu.edu.cn; Fax: +86-771-3233718.

Authors

Shuyan Zhao − *School of Chemistry and Chemical Engineering, Guangxi University, Nanning, Guangxi 530004, P. R. China*

Qianan Zhang − *School of Chemistry and Chemical Engineering, Guangxi University, Nanning, Guangxi 530004, P. R. China*

Yinglan Huang − *School of Chemistry and Chemical Engineering, Guangxi University, Nanning, Guangxi 530004, P. R. China*

Fuhou Lei − *Guangxi Key Laboratory of Chemistry and Engineering of Forest Products, Guangxi Collaborative Innovation Center for Chemistry and Engineering of Forest Products, Guangxi University for Nationalities, Nanning, Guangxi 530006, China*

Complete contact information is available at: https://pubs.acs.org/10.1021/acsomega.1c00217

Notes

The authors declare no competing financial interest.

■ ACKNOWLEDGMENTS

This work was financially supported by the National Natural Science Foundation of China (no. 31870556) and the Open Fund of Guangxi Key Laboratory of Chemistry and Engineering of Forest Products (no. GXFK2001). The authors are grateful to the State Key Laboratory of Element-Organic Chemistry, Nankai University, China, for the bioassay test.

■ REFERENCES

(1) Gu, L. L.; Bai, Y. L. Application and development of 10 kinds of new pesticides with potential. *Mod. Agrochem.* **2018**, *17*, 1−7.

(2) Qiu, S. S.; Bai, Y. L. Progress on research and development of succinate dehydrogenase inhibitor fungicides (I). *Mod. Agrochem.* **2014**, *13*, 1−7.

(3) Liu, X. H.; Qiao, L.; Zhai, Z. W.; Cai, P. P.; Cantrell, C. L.; Tan, C. X.; Weng, J. Q.; Han, L.; Wu, H. K. Novel 4-pyrazole carboxamide derivatives containing flexible chain motif: design, synthesis and antifungal activity. *Pest Manage. Sci.* **2019**, *75*, 2892−2900.

(4) Yang, D.; Zhao, B.; Fan, Z.; Yu, B.; Zhang, N.; Li, Z.; Zhu, Y.; Zhou, J.; Kalinina, T. A.; Glukhareva, T. V. Synthesis and biological activity of novel succinate dehydrogenase inhibitor derivatives as potent fungicide candidates. *J. Agric. Food Chem.* **2019**, *67*, 13185−13194.

(5) Ren, Z.-L.; Liu, H.; Jiao, D.; Hu, H.-T.; Wang, W.; Gong, J.-X.; Wang, A.-L.; Cao, H.-Q.; Lv, X.-H. Design, synthesis, and antifungal activity of novel cinnamon-pyrazole carboxamide derivatives. *Drug Dev. Res.* **2018**, *79*, 307−312.

(6) Du, S.; Li, Z. H.; Tian, Z. M.; Xu, L. Synthesis, antifungal activity and QSAR of novel pyrazole amides as succinate dehydrogenase inhibitors. *Heterocycles* **2018**, *96*, 74−85.

(7) Xiong, L.; Li, H.; Jiang, L.-N.; Ge, J.-M.; Yang, W.-C.; Zhu, X. L.; Yang, G.-F. Structure-based discovery of potential fungicides as succinate ubiquinone oxidoreductase inhibitors. *J. Agric. Food Chem.* **2017**, *65*, 1021−1029.

(8) Yao, T.-T.; Xiao, D.-X.; Li, Z.-S.; Cheng, J.-L.; Fang, S.-W.; Du, Y.-J.; Zhao, J.-H.; Dong, X.-W.; Zhu, G.-N. Design, synthesis, and fungicidal evaluation of novel pyrazole-furan and pyrazole-pyrrole carboxamide as succinate dehydrogenase inhibitors. *J. Agric. Food Chem.* **2017**, *65*, 5397−5403.

(9) Wu, Y.-Y.; Shao, W.-B.; Zhu, J.-J.; Long, Z.-Q.; Liu, L.-W.; Wang, P.-Y.; Li, Z.; Yang, S. Novel 1,3,4-oxadiazole-2-carbohydrazides as prospective agricultural antifungal agents potentially targeting succinate dehydrogenase. *J. Agric. Food Chem.* **2019**, *67*, 13892−13903.

(10) Cheng, H.; Shen, Y.-Q.; Pan, X.-Y.; Hou, Y.-P.; Wu, Q.-Y.; Yang, G.-F. Discovery of 1,2,4-triazole-1,3- disulfonamides as dual inhibitors of mitochondrial complex II and complex III. *New J. Chem.* **2015**, *39*, 7281−7292.

(11) Saraste, M. Oxidative phosphorylation at the fin de siècle. *Science* **1999**, *283*, 1488−1493.

(12) Sun, F.; Huo, X.; Zhai, Y.; Wang, A.; Xu, J.; Su, D.; Bartlam, M.; Rao, Z. Crystal structure of mitochondrial respiratory membrane protein complex II. *Cell* **2005**, *121*, 1043−1057.

(13) Zhu, X.-L.; Xiong, L.; Li, H.; Song, X.-Y.; Liu, J.-J.; Yang, G.-F. Computational and experimental insight into the molecular mechanism of carboxamide inhibitors of succinate-ubquinone oxidoreductase. *ChemMedChem* **2014**, *9*, 1512−1521.

(14) Shang, J.; Sun, R. F.; Li, Y. Q.; Huang, R. Q.; Bi, F. C.; Wang, Q. M. Synthesis and insecticidal evaluation of N - tert - Butyl - N′ - thio [1- (6 - chloro - 3 - pyridylmethyl)-2-nitroiminoimidazolidine]- N, N′-diacylhydrazines. *J. Agric. Food Chem.* **2010**, *58*, 1834−1837.

(15) Tan, Y.; He, H. Q.; Liu, X. H.; Weng, J. Q.; Tan, C. X. Synthesis and herbicidal activities of novel pyridine substituted pyrazole diacylhydrazine derivatives. *Chin. J. Synth. Chem.* **2018**, *26*, 727−732.
(16) Wu, W. N.; Wang, R.; Du, B.; Ouyang, G. P. Synthesis and fungicidal activity evaluation of diacylhydrazine derivatives containing pyrimidine moiety. *Chem. Res. Appl.* **2017**, *29*, 810−815.
(17) Seow, H. A.; Penketh, P. G.; Shyam, K.; Rockwell, S.; Sartorelli, A. C. 1,2-Bis (methylsulfonyl)-1-(2-chloroethyl)-2-[[1-(4-nitrophenyl)ethoxy]carbonyl] hydrazine: an anticancer agent targeting hypoxic cells. *Proc. Natl. Acad. Sci. U.S.A* **2005**, *102*, 9282−9287.
(18) Ajani, O. O.; Obafemi, C. A.; Nwinyi, O. C.; Akinpelu, D. A. Microwave assisted synthesis and antimicrobial activity of 2-quinoxalinone-3-hydrazone derivatives. *Bioorg. Med. Chem.* **2010**, *18*, 214−221.
(19) Boss, C.; Corminboeuf, O.; Grisostomi, C.; Weller, T. Inhibitors of aspartic proteases-potential antimalarial agents. *Expert Opin. Ther. Pat.* **2006**, *16*, 295−317.
(20) Efenberger-Szmechtyk, M.; Nowak, A.; Czyzowska, A.; Kucharska, A. Z.; Fecka, I. Composition and antibacterial activity of Aronia melanocarpa (Michx.) Elliot, Cornus mas L. and Chaenomeles superba Lindl. leaf extracts. *Molecules* **2020**, *25*, 2011.
(21) Spréa, R. M.; Fernandes, Â.; Calhelha, R. C.; Pereira, C.; Pires, T. C. S. P.; Alves, M. J.; Canan, C.; Barros, L.; Amaral, J. S.; Ferreira, I. C. F. R. Chemical and bioactive characterization of the aromatic plant Levisticum officinale W.D.J. Koch: a comprehensive study. *Food Funct.* **2020**, *11*, 1292−1303.
(22) Han, Y. P.; Gong, P.; Li, K. Y. Study on antibacterial activity of phenol hydroxyl from N-aryl Schiff COS derivatives. *Food Mach.* **2015**, *31*, 127−131.
(23) Min, D.; Zhao, J.; Chen, Y.; Zhao, Z. D. Research progress of main sesquiterpenes from heavy turpentine. *Biomass Chem. Eng.* **2017**, *51*, 54−60.
(24) Tyagi, B.; Mishra, M. K.; Jasra, R. V. Solvent free synthesis of 7-isopropyl-1, 1-dimethyltetralin by the rearrangement of longifolene using nano-crystalline sulfated zirconia catalyst. *J. Mol. Catal. A: Chem.* **2009**, *301*, 67−78.
(25) Liu, Z.; Jin, S.; Wang, C.; Zhu, L.; Cheng, Z.; An, X.; Wang, S.; Cai, Z. Synthesis of new tetralin-type musky compounds. *Chem. Ind. For. Prod.* **1995**, *15*, 7−12.
(26) Zhu, X.-P.; Lin, G.-S.; Duan, W.-G.; Li, Q.-M.; Li, F.-Y.; Lu, S.-Z. Synthesis and antiproliferative evaluation of novel longifolene-derived tetralone derivatives bearing 1,2,4-triazole moiety. *Molecules* **2020**, *25*, 986−998.
(27) Lin, G.; Bai, X.; Duan, W.; Cen, B.; Huang, M.; Lu, S. High value-added application of sustainable natural forest product α-pinene: synthesis of myrtenal oxime esters as potential KARI inhibitors. *ACS Sustain. Chem. Eng.* **2019**, *7*, 7862−7868.
(28) Kang, G.-Q.; Duan, W.-G.; Lin, G.-S.; Yu, Y.-P.; Wang, X.-Y.; Lu, S.-Z. Synthesis of bioactive compounds from 3-carene (II): synthesis, antifungal activity and 3D-QSAR study of (Z)- and (E)-3-caren-5-one oxime sulfonates. *Molecules* **2019**, *24*, 477−491.
(29) Lin, G.; Chen, Z.; Duan, W.; Wang, X.; Lei, F. Synthesis and biological activity of novel myrtenal-derived 2-acyl-1,2,4-triazole-3-thione compounds. *Chin. J. Org. Chem.* **2018**, *38*, 2085−2092.
(30) Lin, G.-S.; Duan, W.-G.; Yang, L.-X.; Huang, M.; Lei, F.-H. Synthesis and antifungal activity of novel myrtenal-based 4-methyl-1,2,4-triazole-thioethers. *Molecules* **2017**, *22*, 193−203.
(31) Su, N.-N.; Li, Y.; Yu, S.-J.; Zhang, X.; Liu, X.-H.; Zhao, W.-G. Microwave-assisted synthesis of some novel 1, 2, 3-triazoles by click chemistry, and their biological activity. *Res. Chem. Intermed.* **2013**, *39*, 759−766.
(32) Liu, X.-H.; Shi, Y.-X.; Ma, Y.; Zhang, C.-Y.; Dong, W.-L.; Pan, L.; Wang, B.-L.; Li, B.-J.; Li, Z.-M. Synthesis, antifungal activities and 3D-QSAR study of N-(5-substituted-1,3,4-thiadiazol-2-yl)-cyclopropanecarboxamides. *Eur. J. Med. Chem.* **2009**, *44*, 2782−2786.
(33) Wang, B.-L.; Shi, Y.-X.; Zhang, S.-J.; Ma, Y.; Wang, H.-X.; Zhang, L.-Y.; Wei, W.; Liu, X.-H.; Li, Y.-H.; Li, Z.-M.; Li, B.-J. Syntheses, biological activities and SAR studies of novel carboxamide compounds containing piperazine and arylsulfonyl moieties. *Eur. J. Med. Chem.* **2016**, *117*, 167−178.
(34) Sanner, M. F. Python: a programming language for software integration and development. *J. Mol. Graph. Model.* **1999**, *17*, 57−61.
(35) Sun, N.-B.; Fu, J.-Q.; Weng, J.-Q.; Jin, J.-Z.; Tan, C.-X.; Liu, X.-H. Microwave assisted synthesis, antifungal activity and DFT theoretical study of some novel 1,2,4-triazole derivatives containing the 1,2,3-thiadiazole moiety. *Molecules* **2013**, *18*, 12725−12739.
(36) Frisch, M. J.; Trucks, G. W.; Schlegel, H. B.; Scuseria, G. E.; Robb, M. A.; Cheeseman, J. R.; Scalmani, G.; Barone, V.; Mennucci, B.; Petersson, G. A.; Nakatsuji, H.; Caricato, M.; Li, X.; Hratchian, H. P.; Izmaylov, A. F.; Bloino, J.; Zheng, G.; Sonnenberg, J. L.; Hada, M.; Ehara, M.; Toyota, K.; Fukuda, R.; Hasegawa, J.; Ishida, M.; Nakajima, T.; Honda, Y.; Kitao, O.; Nakai, H.; Vreven, T.; Montgomery, J. A., Jr.; Peralta, J. E.; Ogliaro, F.; Bearpark, M.; Heyd, J. J.; Brothers, E.; Kudin, K. N.; Staroverov, V. N.; Kobayashi, R.; Normand, J.; Raghavachari, K.; Rendell, A.; Burant, J. C.; Iyengar, S. S.; Tomasi, J.; Cossi, M.; Rega, N.; Millam, J. M.; Klene, M.; Knox, J. E.; Cross, J. B.; Bakken, V.; Adamo, C.; Jaramillo, J.; Gomperts, R.; Stratmann, R. E.; Yazyev, O.; Austin, A. J.; Cammi, R.; Pomelli, C.; Ochterski, J. W.; Martin, R. L.; Morokuma, K.; Zakrzewski, V. G.; Voth, G. A.; Salvador, P.; Dannenberg, J. J.; Dapprich, S.; Daniels, A. D.; Farkas, Ö.; Foresman, J. B.; Ortiz, J. V.; Cioslowski, J.; Fox, D. J. *Gaussian 09*; Gaussian, Inc.: Wallingford, CT, 2009.
(37) Dennington, R.; Keith, T.; Millam, J. *GaussView*, Version 5; Semichem, Inc.: Shawnee Mission, KS, 2009.

https://doi.org/10.1021/acsomega.1c00217
ACS Omega 2021, 6, 9104−9111